Slow-light, band-edge waveguides for tunable time delays

M. L. Povinelli, Steven G. Johnson, J. D. Joannopoulos

Department of Physics and the Center for Materials Science and Engineering, Massachusetts Institute of Technology, 77 Massachusetts Avenue, Cambridge, Massachusetts 02139

mpovinel@alum.mit.edu

Abstract: We propose the use of slow-light, band-edge waveguides for compact, integrated, tunable optical time delays. We show that slow group velocities at the photonic band edge give rise to large changes in time delay for small changes in refractive index, thereby shrinking device size. Figures of merit are introduced to quantify the sensitivity, as well as the accompanying signal degradation due to dispersion. It is shown that exact calculations of the figures of merit for a realistic, three-dimensional grating structure are well predicted by a simple quadratic-band model, simplifying device design. We present adiabatic taper designs that attain $<0.1\%$ reflection in short lengths of 10 to 20 times the grating period. We show further that cascading two gratings compensates for signal dispersion and gives rise to a constant tunable time delay across bandwidths greater than 100 GHz. Given typical loss values for silicon-on-insulator waveguides, we estimate that gratings can be designed to exhibit tunable delays in the picosecond range using current fabrication technology.

OCIS codes: (130.3120) Integrated optics devices; (130.2790) Guided waves

References and links

1. G. Lenz, B. J. Eggleton, C. K. Madsen, and R. E. Slusher, "Optical delay lines based on optical filters," IEEE J. Quantum Electron. **37**, 525–532 (2001).
2. R. Ramaswami and K. N. Sivarajan, *Optical Networks: A Practical Perspective* (Academic Press, London, 1998).
3. M. S. Rasras, C. K. Madsen, M. A. Cappuzzo, E. Chen, L. T. Gomez, E. J. Laskowski, A. Griffin, A. Wong-Foy, A. Gasparyan, A. Kasper, J. LeGrange, and S. S. Patel, "Integrated resonance-enhanced variable delay lines," IEEE Photonics Technol. Lett. **17**, 834–6 (2005).
4. Z. Wang and S. Fan, "Compact all-pass filters in photonic crystals as the building block for high-capacity optical delay lines," Phys. Rev. E **68**, 066,616 (2003).
5. A. Yariv, Y. Xu, R. K. Lee, and A. Scherer, "Coupled-resonator optical waveguide: a proposal and analysis," Opt. Lett. **24**, 711–713 (1999).
6. S. Mookherjea and A. Yariv, "Coupled Resonator Optical Waveguides," IEEE J. Sel. Top. Quantum Electron. **8**, 448–456 (2002).
7. J. Liu, B. Shi, D. Zhao, and X. Wang, "Optical delay in defective photonic bandgap structures," J. Opt. A.: Pure Appl. Opt. **4**, 636–639 (2002).
8. S. Nishikawa, S. Lan, N. Ikeda, Y. Sugimoto, H. Ishikawa, and K. Asakawa, "Optical characterization of photonic crystal delay lines based on one-dimensional coupled defects," Opt. Lett. **27**, 2079–2081 (2004).
9. H. Altug and J. Vučković, "Two-dimensional coupled photonic crystal resonator arrays," Appl. Phys. Lett. **84**, 161–163 (2004).
10. H. Altug and J. Vučković, "Experimental demonstration of the slow group velocity of light in two-dimensional coupled photonic crystal microcavity arrays," Appl. Phys. Lett. **86**, 111,102 (2005).
11. M. F. Yanik and S. Fan, "Stopping light all optically," Phys. Rev. Lett. **92**, 083,901 (2004).
12. M. F. Yanik, W. Suh, Z. Wang, and S. Fan, "Stopping Light in a Waveguide with an All-Optical Analog of Electromagnetically Induced Transparency," Phys. Rev. Lett. **93**, 233,903 (2004).

#8019 - $15.00 USD Received 6 July 2005; revised 24 August 2005; accepted 29 August 2005

13. D. D. Smith, H. Chang, K. A. Fuller, A. T. Rosenberger, and R. W. Boyd, "Coupled-resonator-induced transparency," Phys. Rev. A **69**, 063,804 (2004).
14. M. Scalora, R. J. Flynn, S. B. Reinhardt, R. L. Fork, M. J. Bloemer, M. D. Tocci, C. M. Bowden, H. S. Ledbetter, J. M. Bendickson, and R. P. Leavitt, "Ultrashort pulse propagation at the photonic band edge: Large tunable group delay with minimal distortion and loss," Phys. Rev. E **54**(2), R1078–1081 (1996).
15. D. Mori and T. Baba, "Dispersion-contolled optical group delay device by chirped photonic crystal waveguides," Appl. Phys. Lett. **85**, 1101–1103 (2004).
16. J. D. Joannopoulos, R. D. Meade, and J. N. Winn, *Photonic Crystals: Molding the Flow of Light* (Princeton Univ. Press, 1995).
17. S. G. Johnson, P. Bienstman, M. A. Skorobogatiy, M. Ibanescu, E. Lidorikis, and J. D. Joannopoulos, "Adiabatic theorem and continuous coupled-mode theory for efficient taper transitions in photonic crystals," Phys. Rev. E **66**, 066,608 (2002).
18. M. I. Skolnik, *Introduction to Radar Systems*, chap. 11.5 (McGraw-Hill, 1980).
19. J. T. Hastings, M. H. Lim, J. G. Goodberlet, and H. I. Smith, "Optical waveguides with apodized sidewall gratings via spatial-phase locked electron-beam lithography," J. Vac. Sci. Technol. B **20**, 2753–2757 (2002).
20. G. E. Jellison and H. H. Burke, "The temperature depdendence of the refractive index of silicon at elevated temperatures at several laser wavelengths," J. Appl. Phys. **60**, 841–843 (1986).
21. S. G. Johnson and J. D. Joannopoulos, "Block-iterative frequency-domain methods for Maxwell's equations in a planewave basis," Opt. Express **8**, 173–190 (2001). http://www.opticsexpress.org/abstract.cfm?URI=OPEX-8-3-173.
22. J. S. Foresi, P. R. Villeneuve, J. Ferrera, E. R. Thoen, G. Steinmeyer, S. Fan, J. D. Joannopoulos, L. C. Kimerling, H. I. Smith, and E. P. Ippen, "Photonic-bandgap microcavities in optical waveguides," Nature **390**, 143–145 (1997).
23. S. G. Johnson, M. L. Povinelli, P. Bienstman, M. Skorobogatiy, M. Soljačić, M. Ibanescu, E. Lidorikis, and J. D. Joannopoulos, "Coupling, scattering and perturbation theory: Semi-analytical analyses of photonic-crystal waveguides," in *Proc. 2003 5th Intl. Conf. on Transparent Optical Networks and 2nd Eur opean Symp. on Photonic Crystals*, vol. 1, pp. 103–109 (2003).
24. N. M. Litchinitser, B. J. Eggleton, and G. P. Agrawal, "Dispersion of Cascaded Fiber Gratings in WDM Lightwave Systems," J. Lightwave Technol. **16**, 1523–9 (1998).
25. M. Soljačić, E. Lidorikis, L. V. Hau, and J. D. Joannopoulos, "Enhancement of microcavity lifetimes using highly dispersive materials," Phys. Rev. E **71**, 026602 (2005).
26. M. Skorobogatiy, G. Bégin, and A. Talneau, "Statistical analysis of geometrical imperfections from the images of 2D photonic crystals," Opt. Express **13**, 2487–2502 (2005).
27. M. L. Povinelli, S. G. Johnson, E. Lidorikis, J. D. Joannopoulos, and M. Soljačić, "Effect of a photonic bandgap on scattering from waveguide disorder," Appl. Phys. Lett. **84**, 3639–3641 (2004).
28. S. G. Johnson, M. L. Povinelli, M. Soljačić, A. Karalis, S. Jacobs, and J. D. Joannopoulos, "Roughness losses and volume-current methods in photonic-crystal waveguides," J. Appl. Phys. B **81**(2–3), 283–293 (2005).
29. S. Hughes, L. Ramunno, J. F. Young, and J. E. Sipe, "Extrinsic optical scattering loss in photonic crystal waveguides: role of fabrication disorder and photon group velocity," Phys. Rev. Lett. **94**, 033,903 (2005).
30. M. Notomi, A. Shinya, S. Mitsugi, E. Kuramochi, and H.-Y. Ryu, "Waveguides, resonators, and their coupled elements in photonic crystal slabs," Opt. Express **12**, 1551–1561 (2004). http://www.opticsexpress.org/abstract.cfm?URI=OPEX-12-8-1551.
31. K. K. Lee, D. R. Lim, L. C. Kimerling, J. Shin, and F. Cerrina, "Fabrication of ultralow-loss Si/SiO_2 waveguides by roughness reduction," Opt. Lett. **26**, 1888–1890 (2001).
32. F. Grillot, L. Vivien, S. Laval, S. Pascal, and E. Cassan, "Size Influence on the Propagation Loss Induced by Sidewall Roughness in Ultrasmall SOI Waveguides," IEEE Photonics Technol. Lett. **16**, 1661–1663 (2004).
33. Y. Akahane, T. Asano, B.-S. Song, and S. Noda, "Fine-tuned high-Q photonic-crystal nanocavity," Opt. Express **13**, 1202–1214 (2005).
34. J. Niehusmann, A. Vörckel, P. H. Bolivar, T. Wahlbrink, W. Henschel, and H. Kurz, "Ultrahigh-quality-factor silicon-on-insulator microring resonator," Opt. Lett. **29**, 2861–2863 (2004).
35. S. J. Spector, M. W. Geis, and T. Lyszczarz. Private communication.

1. Introduction

Delaying an optical signal is useful for a number of applications, including optical buffering, signal processing, logic, and radio-frequency (RF) photonics [1]. Several recent research efforts have focused on replacing relatively bulky fiber-optic delay-line systems [2] with compact integrated devices. Approaches have included the use of all-pass filters [1, 3, 4] and coupled-resonator optical waveguides [5, 6, 7, 8, 9, 10, 11, 12, 13]. Such devices are ultimately limited by the resonator quality factor Q. Moreover, *tuning* the time-delay typically requires precise

#8019 - $15.00 USD Received 6 July 2005; revised 24 August 2005; accepted 29 August 2005

spatial control over the thermal, optical, or electric control fields.

Here, we examine an alternative approach to tunable, integrated time delays: slow-light, band-edge photonic-crystal waveguides. Previous work in ideal, 1-D structures has suggested that near a photonic band edge, a large delay tunability can be achieved for a small change in refractive index [14]. We investigate this slow-light enhancement phenomenon in realistic, three-dimensional structures amenable to on-chip fabrication using established lithographic techniques. In contrast to other work [15], we use a single waveguide through which light is transmitted at slow speeds near the band edge, rather than a structure in which light is reflected from the band edge or transferred to another waveguide. By adiabatically tapering the grating, we simultaneously achieve high transmission and large tunable delays. Moreover, we show that cascading two such tapered gratings gives a flat tunable time delay across large operating bandwidths $>$100 GHZ. Since the tuning mechanism relies only on the bulk properties of the gratings, the need for spatial control/positioning of the tuning fields is minimized.

The outline of the paper is as follows. In Sects. 2 and 3 we describe the principle of operation of our device and introduce relevant figures of merit to describe tunable time delays, namely sensitivity, length, and dispersion. We then introduce a quadratic band model to predict the dependence of the figures of merit on distance from the band edge and grating strength in Sect. 4. The validity of the quadratic band model is demonstrated by explicit comparison to calculations for a realistic, three-dimensional structure in Sect. 5, simplifying device design and optimization. Sect. 6 discusses the design of adiabatic tapers connecting slow-light, band-edge waveguides with uniform waveguide regions. A semi-analytical, coupled-mode theory approach is used to optimize the taper rate, achieving low reflection in short lengths. Sect. 7 illustrates how two adiabatically tapered gratings can be cascaded to compensate for dispersion near the band edge. Using the quadratic band model, we show that nearly-flat time delays can be achieved across the operating bandwidth. The value of the tunable delay will increase as the operating frequency approaches the band edge. In Sect. 8, we estimate the achievable tunable delay given current fabrication techniques. The role of fabrication tolerances and waveguide loss is discussed, including the effect of slow light speeds on loss scaling. Our analysis shows that obtaining tunable time delays greater than tens of picoseconds by band-edge gratings alone imposes increasingly challenging waveguide-loss requirements. Sect. 9 comments on similarities and differences to resonator-based time delays, and Sect. 10 summarizes our results.

2. Principle of Operation

We begin by describing the principle of operation of our slow-light, band-edge tunable time delay device. A wide variety of 1-, 2-, and 3-D periodic, dielectric structures have dispersion relations with zero group velocity at the edge of the Brillouin zone [16]. Here we will focus on 1-D periodic gratings with finite width and height, such as those shown in Fig. 1(a), which can be relatively easily integrated on-chip. A grating may be made, for example, by etching teeth in the side of the waveguide, grooves in its top surface, or holes spaced along its length. Such gratings have band structures with the general features shown in Fig. 1(b). The light cone region indicates modes that are extended in either the air or the substrate and is shaded grey. Guided modes of the grating are plotted as solid lines and specified by a frequency ω and a wave vector k along the waveguide axis. A range of typical 1-D periodic structures exhibit a band gap (shaded yellow) in the guided modes lying below the light line. At the edge of the band gap, the group velocity $d\omega/dk$ of a guided mode goes to zero. Figure 1(c) shows a magnified view of this region. A small shift in refractive index from n to n', induced for example by thermal, optical, or electrical tuning, will cause a small shift in the band. For constant operating frequency, indicated by the horizontal dotted line, a large change in group velocity can result. A large change in group velocity corresponds to a large change in the time required to propagate

#8019 - $15.00 USD Received 6 July 2005; revised 24 August 2005; accepted 29 August 2005

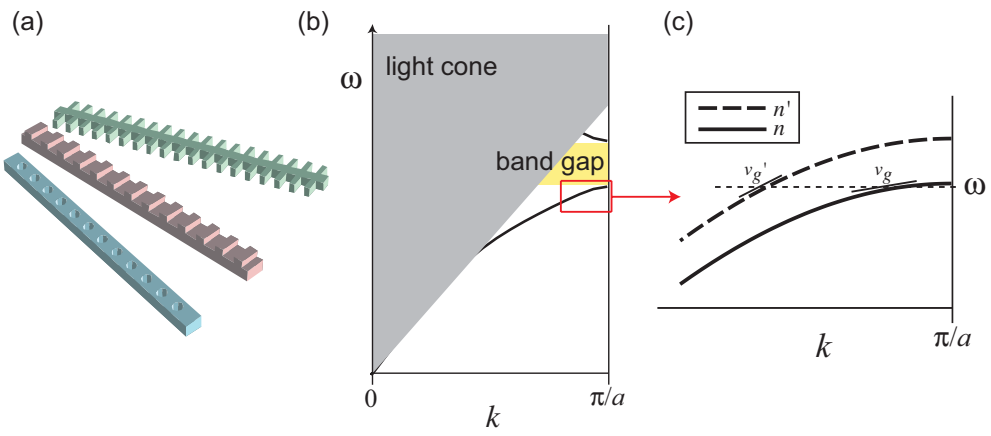

Fig. 1. (a) Types of 1-D periodic gratings. (b) Typical band structure of a 1-D periodic grating. The band gap is shaded yellow. (c) Magnified view of the band structure near the band edge, illustrating how a small shift in refractive index can lead to a large shift in group velocity. (The case shown corresponds to $n' < n$, or $\Delta n < 0$.)

through a fixed length of grating, and hence a highly-tunable time delay.

The transmission through any finite-length grating depends not only on the band structure, but also on reflection and loss from the ends of the grating. However, the magnitude of such effects can be made arbitrarily small by appropriate tapering, as proved rigorously in [17]. We first examine useful figures of merit determined from the band structure of the device alone. Later in Section 6, we explicitly demonstrate a low-reflection taper design for an optimized grating.

3. Figures of Merit

We introduce three figures of merit useful for characterizing any tunable time-delay device. It is convenient to define the figures of merit in terms of the maximum, achievable index shift, Δn, and the resulting change in delay, $\Delta\tau$, that would typically be measured in an experiment.

The first is the *sensitivity*, a dimensionless figure of merit given by the fractional change in time delay over the fractional change in index:

$$s \equiv \frac{\Delta\tau/\tau}{\Delta n/n} = \frac{\Delta(1/v_g)_{\Delta n}}{1/v_g}\frac{1}{\Delta n/n}, \tag{1}$$

where τ is the time delay, v_g is the waveguide group velocity, and $\Delta(1/v_g)_{\Delta n} = 1/v_g' - 1/v_g$ is the change in inverse group velocity due to a shift from n to $n' = n + \Delta n$. s indicates the advantage of the slow-light waveguide structure as compared to a bulk material. For bulk, $\omega = ck/n$ and $s = 1$.

For a fixed fractional index shift $\Delta n/n$ and a desired tunable delay $\Delta\tau$, the required length is given by

$$L = \left|\frac{\Delta\tau}{\Delta(1/v_g)_{\Delta n}}\right| = \left|\frac{\Delta\tau}{\Delta n/n}\frac{v_g}{s}\right|. \tag{2}$$

Waveguides with low group velocity and high sensitivity allow a shorter tuning region, leading to lower power and ease of integration.

Sensitivity is high near the band edge because of group-velocity dispersion $(d^2\omega/dk^2 \neq 0)$, but dispersion can also limit the performance of the device. It is useful to define a *dispersion*

#8019 - $15.00 USD Received 6 July 2005; revised 24 August 2005; accepted 29 August 2005

figure of merit to measure the amount of pulse spreading relative to the typical size $1/\Delta\omega$ of temporal features (e.g. pulses or chirp autocorrelations [18]), where $\Delta\omega$ is the bandwidth.

$$d \equiv \frac{\tau|_{\omega} - \tau|_{\omega-\Delta\omega}}{1/\Delta\omega} = \frac{L\Delta(1/v_g)_{\Delta\omega}}{1/\Delta\omega} \tag{3}$$

where $\Delta(1/v_g)_{\Delta\omega} \equiv \frac{1}{v_g}\Big|_{\omega} - \frac{1}{v_g}\Big|_{\omega-\Delta\omega}$ is the change in inverse group velocity across the bandwidth. Making use of Eq. 2, d may alternatively be written as

$$d = |\Delta\tau|\Delta\omega \frac{\Delta(1/v_g)_{\Delta\omega}}{\left|\Delta(1/v_g)_{\Delta n}\right|}. \tag{4}$$

4. Quadratic Band Model

We next use an approximate model for the dispersion relation near the band edge to yield useful approximations for the figures of merit above. Near the band edge ω_{be}, $\omega(k)$ can be approximated by a quadratic curve,

$$\omega(k) = \omega_{\mathrm{be}} - \alpha(\pi/a - k)^2,$$

where $\alpha = -\frac{1}{2}\, d^2\omega/dk^2\big|_{\pi/a}$. Large values of α correspond to large curvature of the band structure: the group velocity changes from a large, non-zero value to zero over a small frequency range. Such behavior is characteristic of weak gratings, which have a small band gap. Strong gratings, which have larger band gaps, have small values of α.

The shifted band may similarly be written as

$$\omega'(k) = \omega_{\mathrm{be}} + \delta\omega - (\alpha + \delta\alpha)(\pi/a - k)^2.$$

Let $\Delta\omega_{\mathrm{be}} \equiv \omega_{\mathrm{be}} - \omega$. Then

$$s \approx -\frac{1}{\Delta n/n}\left(1 - \frac{1}{\sqrt{(1+\delta\omega/\Delta\omega_{\mathrm{be}})(1+\delta\alpha/\alpha)}}\right). \tag{5}$$

As the operating frequency approaches the band edge, $|s|$ increases until it reaches a limiting value of $|n/\Delta n|$.[1] This behavior can be interpreted as a signature of slow-light enhancement of the time-delay tunability, since s increases with decreasing v_g.

The length is given by

$$L \approx \left|\frac{2\Delta\tau\sqrt{\alpha\Delta\omega_{\mathrm{be}}}}{1 - [(1+\delta\omega/\Delta\omega_{\mathrm{be}})(1+\delta\alpha/\alpha)]^{-1/2}}\right|. \tag{6}$$

L decreases to zero near the band edge, scaling as $L = 2|\Delta\tau(\alpha\Delta\omega_{\mathrm{be}})^{1/2}|$ for $|\Delta\omega_{\mathrm{be}}| \ll |\delta\omega|$. For a given, desired time delay and a fixed distance from the band edge, small α (corresponding to strong gratings) give the shortest device lengths.

The dispersion figure of merit is approximated by

$$d \approx \frac{L\Delta\omega}{2\sqrt{\alpha}}\left[\frac{1}{\sqrt{\Delta\omega_{\mathrm{be}}}} - \frac{1}{\sqrt{\Delta\omega_{\mathrm{be}} + \Delta\omega}}\right]. \tag{7}$$

[1] We note that approximating s with a partial derivative with respect to n would incorrectly give a divergent value at the band edge; the sensitivity is in fact finite at the band edge for finite Δn.

#8019 - $15.00 USD Received 6 July 2005; revised 24 August 2005; accepted 29 August 2005

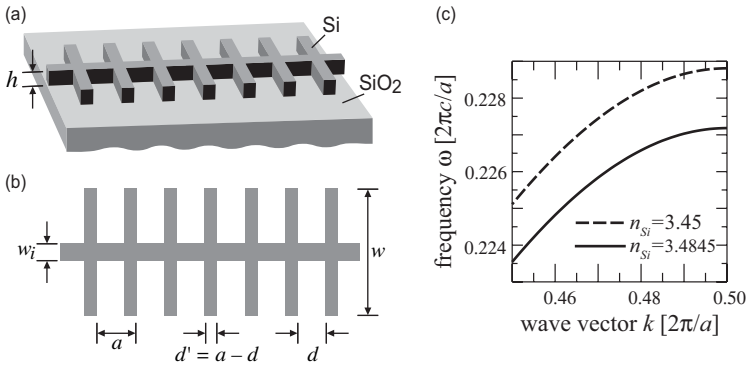

Fig. 2. (a) 3-D perspective view of a slow-light grating structure. (b) Top view. (c) Band structure.

Because L scales as $\sqrt{\alpha}$ (up to small corrections that are first order in $\delta\alpha/\alpha \propto \Delta n/n$), d is nearly independent of α within the quadratic band model. Approaching the band edge, dispersion increases to a limiting value of $|\Delta\tau|\Delta\omega$. This quantity can be interpreted as a *tunable delay*-bandwidth product. Specifying an allowable dispersive spread limits the achievable time delay for a given bandwidth. At the band edge, this limit takes the form $|\Delta\tau| < d/\Delta\omega$.

We note that in general, the values of s and L depend on the available tunable index shift, $\Delta n/n$. For this reason, different device designs should be compared using a fixed $\Delta n/n$ value. However, the quadratic band model expressions above show that L is independent of the index shift for frequencies sufficiently close to the band edge. The dispersion figure of merit d is also independent of the index shift, since it is defined entirely in terms of the unshifted band, for which the operating frequency is closest to the band edge and the dispersive effects are most significant.

5. Numerical Results

To explicitly verify the utility of the quadratic band model, we present exact numerical results for the figures of merit for a realistic slow-light structure. We consider the structure shown in Fig. 2(a) and (b), a silicon strip waveguide with grated sidewalls [19] resting on a silicon-dioxide substrate. Silicon, in particular, has low absorption near 1.55 μm, high refractive index, and large change in index with temperature; the index varies by $>$1% from 100 to 300 ℃ [20].

Sensitivity, length, and dispersion figures of merit were calculated from the dispersion relation of the structure, which was obtained from fully-vectorial solutions of Maxwell's equations in a plane-wave basis [21]. Structural parameters were determined by maximizing the size of the first band gap under the constraint that the minimum feature size be at least 0.15 μm. The parameters are h = 0.26 μm, w_i = 0.15 μm, a = 0.35 μm, d' = 0.15 μm, d = 0.20 μm, and w = 1.0224 μm. For n_{Si} = 3.4845 and $n_{\mathrm{SiO_2}}$ = 1.45, the first band gap was 23.5% of the midgap frequency for odd modes with respect to the mirror plane of the structure ($\vec{E}$ mostly parallel to the substrate). For n_{Si} = 3.4845, the band edge frequency was calculated to be $\omega_{\mathrm{be}} = 0.22718\,[2\pi c/a]$ for the lowest band, or $\omega_{\mathrm{be}}/2\pi$ = 190 THz (λ = 1.54 μm). For n'_{Si} = 3.45 ($\Delta n/n = -0.01$), the band edge shifted to $\omega_{\mathrm{be}} = 0.22880\,[2\pi c/a]$, or $\omega_{\mathrm{be}}/2\pi$ = 200 THz (λ = 1.53 μm). Figure 2(c) shows the lowest band near the band edge.

Figures 3 and 4 show the results of the exact numerical calculation (symbols) overlayed on the expressions for s, L, and d obtained from the quadratic band model of Eqs. 5, 6, and 7 (solid lines). As can be seen from the figure, the quadratic band model is an excellent predictor of the

#8019 - $15.00 USD Received 6 July 2005; revised 24 August 2005; accepted 29 August 2005

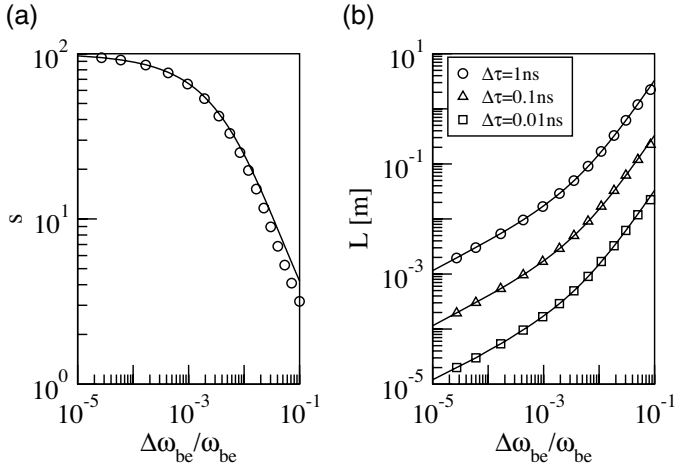

Fig. 3. (a) Sensitivity figure of merit for the structure of Fig. 2 as a function of fractional frequency from the band edge. (b) Required length for different amounts of tunable time delay. Symbols/solid lines are exact/quadratic-approximation calculations for a fractional index shift $\Delta n/n = -0.01$.

results within at least 1% from the band edge. In general, we expect the range of validity of the quadratic band model to decrease as the band gap is decreased. Values of $\delta\omega$ (0.00162[$2\pi c/a$]) and α (1.525[$ca/2\pi$]), and $\delta\alpha$ (0.025[$ca/2\pi$]) were obtained from a fit to the data of Fig. 2(c) at $k = \pi/a$. Fig. 3(a) exhibits the expected increase of s as the operating frequency approaches the band edge (see Eq. 5). Figure 3(b) exhibits the expected linear scaling of L with the required time delay, $\Delta\tau$ (see Eq. 6). From Eq. 7, we expect d to scale linearly with the tunable delay $\Delta\tau$, as shown in Fig. 4(a). The dependence on bandwidth $\Delta\omega$ is more complex, as shown in Fig. 4(b).

To illustrate the utility of the figures of merit, let us consider a tunable time delay of 1 ns. Assuming that we can operate at a frequency 2% away from the band edge, Fig. 3(b) shows that a length of 0.4 m is required. Simple estimates show that meters of grating can easily be fit onto chips with areas less than 0.1 cm^2. For a 1 GHz signal bandwidth, the pulse duration is $\sim$ 1 ns, and the tunable time delay is comparable to the pulse duration. Meanwhile, the dispersive spread may be obtained from Fig. 4(b) and is less than one-hundredth of the pulse width. For a 10 GHz bandwidth, the pulse width is 10 times shorter, and a tunable delay of 1 ns corresponds to 10 times the pulse width. However, the dispersive spread is now comparable to the pulse width. Moving toward larger bandwidths and longer time delays suggests the use of dispersion compensation, as discussed in Section 7 below.

6. Taper Design

Intuitively, coupling power into a slow-light waveguide is difficult because of the large "impedance" mismatch between the slow-light waveguide and a normal waveguide (or free-space propagation). In order to circumvent this, we apply three ideas. First, we exploit the existence of an adiabatic theorem [17]: for a gradual taper satisfying some simple conditions, one can (in principle) approach 100% transmission when coupling two arbitrary periodic or uniform waveguides. Second, we have explicitly chosen a periodic waveguide design that is amenable to a gradual transition to a uniform waveguide: the sidewall protrusions in Fig. 2 can be gradually reduced until they are eliminated, without ever requiring a small feature size or high aspect

#8019 - $15.00 USD Received 6 July 2005; revised 24 August 2005; accepted 29 August 2005

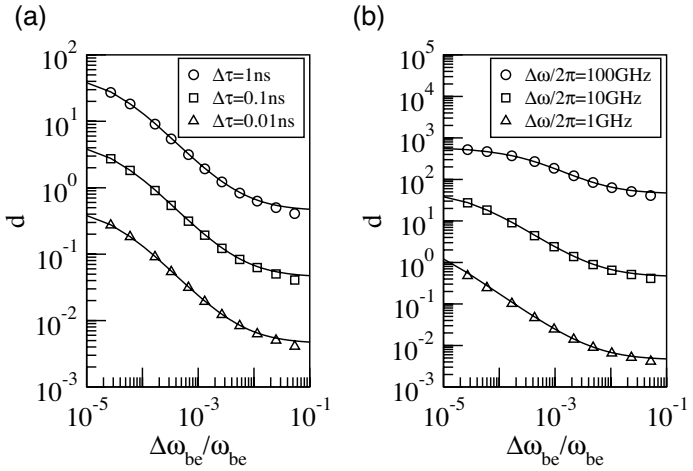

Fig. 4. Dispersion figures of merit for the structure of Fig. 2 as a function of fractional frequency from the band edge for (a) fixed bandwidth $\Delta\omega/2\pi$=10 GHz and (b) fixed time delay $\Delta\tau$=1ns. Symbols/solid lines are exact/quadratic-approximation calculations for a fractional index shift $\Delta n/n = -0.01$.

ratio that would be impractical to fabricate [19]. (This is not true of all periodic waveguides; for example, periodic cylindrical holes [22] could not be gradually removed without facing the difficult prospect of etching very small holes.) Third, we exploit the existence of efficient coupled-mode–theory models of gradual transitions in order to design an optimized transition that uses the slowest rate of change for the lowest-group-velocity regions. In the following, we discuss this design optimization process to show how a taper can achieve 0.1% reflection in only ten periods and 0.001% reflection in 50 periods when coupling to our grated waveguide operating within 2% of the band edge at a group velocity near $0.1c$. We also discuss general scaling laws that make coupling to slow-light waveguides more difficult.

The (fully-vectorial) coupled-mode theory of [17] expands the fields in a tapered waveguide in the basis of the Bloch modes $|n\rangle$ of the perfect periodic waveguide corresponding to the tapered waveguide "at" each position z along the taper. One then obtains a set of ordinary differential "coupled-mode" equations in the expansion coefficients $c_n(z)$. In slow-light waveguides, the scattering is dominated by coupling to the reflected mode, which can be expressed as simple integral in the case of a slow taper. In brief, the amplitude c_r of the reflected mode (normalized so that the reflection coefficient is $|c_r|^2$) for a taper of length L is given to lowest order in the taper rate by:

$$c_r = -\int_0^L dz \sum_k \frac{\left\langle r \left| e^{2\pi i k/a} \frac{\partial \hat{C}}{\partial z} \right| i \right\rangle}{\Delta\beta_k(z)} \times \exp\left[i \int_0^z \Delta\beta_k(z')dz' \right], \tag{8}$$

where the $\langle r|\cdots|i\rangle$ is a geometry-dependent coupling integral proportional to the taper rate $1/L$, and $\Delta\beta_k(z) = \Delta\beta + 2\pi k/a$ is the mismatch between the wavenumber β of the initial mode i and the reflected mode r plus a quasi-phase-matching factor $2\pi k/a$ summed over all integers k (in practice, only k near 0 contribute significantly [17]). Previous comparisons to brute-force simulation in 2d have shown that Eq. (8) is nearly indistinguishable from the exact results once the reflection falls below 10% (i.e., the taper is slow enough). There are two important features of this integral: first, the slow taper rate is handled analytically via the coupling integral (a small computation over the unit cell of the periodic structure), as opposed to a brute-force simula-

#8019 - $15.00 USD Received 6 July 2005; revised 24 August 2005; accepted 29 August 2005

tion which would require a high resolution to capture a small rate of change; and second, the integrands only change by an overall scale factor as the taper rate varies, so one can quickly compute reflection for many different taper lengths L. Thus, we can make quantitative predictions about the reflection in our tapers that would be prohibitive to simulate more directly in 3d.

The reflection coefficient for a 3d "linear" taper where the sidewall protrusions are extended proportional to $(L-z)/L$ is shown in Fig. 5 as a function of L. Note that the reflection spectrum exhibits ripples as a function of taper length. These correspond to Fabry-Perot oscillations of the form $\sin^2(\Delta\beta L/2)$, where $\Delta\beta$ is a characteristic wave vector mismatch between the guided and reflected mode [17]. To good approximation, $\Delta\beta$ is given by $2(k(\omega)-\pi/a)$ of the slow-light grating. A dip of length ΔL at fixed frequency directly corresponds to the frequency range of oscillation $\Delta\omega_{\mathrm{FP}}$ at fixed length L as

$$\frac{\Delta\omega_{\mathrm{FP}}}{\omega} \approx \frac{v_g \Delta L}{2L}\frac{\Delta\beta}{\omega}. \tag{9}$$

Much better performance can be achieved by means of a *variable*, rather than linear, taper. A variable taper rate is attractive because the integrand in Eq. (8) diverges as the group velocity v_g goes to zero, making it important to taper more slowly in low-group velocity regions. In particular, the (fixed-power) normalization of the fields $\langle r|$ and $|i\rangle$ both scale as $1/\sqrt{v_g}$, and the wavenumber mismatch $\Delta\beta$ between forward and backward modes scales proportionally to v_g near a quadratically-shaped band edge. Moreover, the overall reflected power $|c_r|^2$ from Eq. (8) was shown [17] to be approximately $|\langle r|\cdots|i\rangle/\Delta\beta^2|^2$, and thus we find that $|c_r|^2 \sim (1/v_g^3 L)^2$, or that the taper length L for a fixed reflection coefficient must scale as $1/v_g^3$ [23]. For a quadratic band, $v_g \sim \sqrt{\alpha\Delta\omega_{\mathrm{be}}}$ and

$$L \sim \frac{1}{(\alpha\Delta\omega_{\mathrm{be}})^{3/2}}. \tag{10}$$

Not suprisingly, operating closer to the band edge and/or employing a grating with a larger gap (smaller α) tend to increase the required taper length.

We parameterize a variable-taper structure by a position s that goes from 0 at the beginning to 1 at the end of the taper, and by a taper rate $R(s)$ (nonzero in $[0,1]$) normalized so that $1=\int_0^1 ds/R(s)$. Then, in Eq. (8), one simply substitutes $\partial\hat{C}/\partial z\cdot dz = \partial\hat{C}/\partial s\cdot ds$ and $dz' = L\cdot ds'/R(s')$, and the reflection for any $R(s)$ can then be evaluated without recomputing the Bloch modes or coupling integrals. To optimize the taper, we describe $R(s)$ by a degree-4 polynomial in s with unknown coefficients, which are determined by an unconstrained nonlinear minimization of $|c_r|^2$ performed in Matlab. Due to Fabry-Perot effects, optimizing $|c_r|^2$ at a fixed L would result in a sharp interference "dip" that would have narrow bandwidth and be sensitive to perturbations; instead, we perform a minimax optimization to minimize the maximum reflection for L in $[50a, 90a]$.

The result is shown in Fig. 5(a) and demonstrates an improvement by one to two orders of magnitude over the linear taper. We note that obtaining the same result by direct simulation would have required $\sim 10^4$ difficult 3d transmission calculations. The calculation of Fig. 5(a) was performed for $n_{\mathrm{Si}}=3.45$ and $\omega = 0.22491[2\pi c/a]$ (1.7296% from the band edge). At this frequency, $k = 0.44876[2\pi/a]$ and $v_g = 0.10753c$. The optimized taper rate is $R(s) = 8.996477 - 44.691669s + 90.618493s^2 - 74.831399s^3 + 19.941150s^4$. To convert this into width $w_t(z)$ of the gratings along the taper, one must first compute $z(s) = L\int_0^s 1/R(s')ds'$ and then invert it to obtain $w_t(z) = w_i + (w-w_i)\cdot s(z)$ where w_i and w are defined in Fig. 5. (This process to find $w_t(z)$ from $R(s)$ is a matter of two lines in Matlab or similar.) The resulting taper shape, shown in Fig. 5(b), has a rapid increase in grating width at the beginning, followed by nearly linear tapering, followed by a very gradual taper at the end where v_g is small.

#8019 - $15.00 USD Received 6 July 2005; revised 24 August 2005; accepted 29 August 2005

(a)

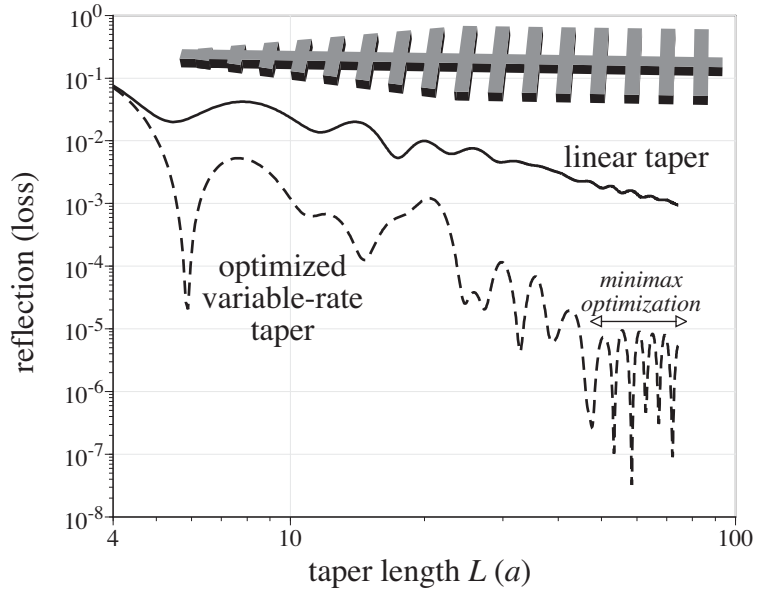

(b)

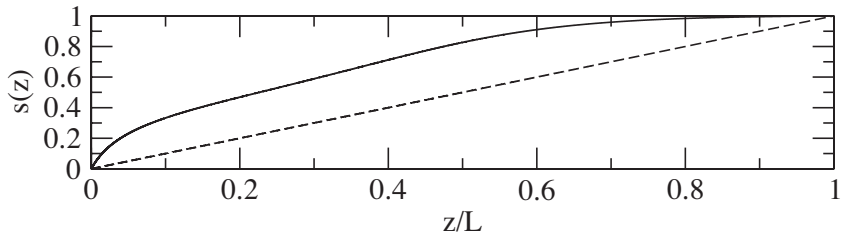

Fig. 5. (a) Reflection as a function of the length of a taper (in units of a, the waveguide period) connecting a uniform waveguide to the grated waveguide of Fig. 2 for $n_{\mathrm{Si}} = 3.45$ and $\omega = 0.22491[2\pi c/a]$ ($< 2\%$ from the band edge). Results were obtained from 3d numerical integration of the coupling integral in Eq. 8. (b) Normalized taper profile $s(z)$ for linear taper (dashed line) and optimized, variable-rate taper (solid line).

Since the optimized taper attains $< 0.1\%$ reflections in short lengths from 10–20a, which is much smaller than the overall length of the delay design, we are justified in neglecting the taper coupler's effects on group delay and dispersion in our device. In general, the taper should be designed for the edge of bandwidth closest to to the band edge, for which the required length is greatest. Further from the band edge, the reflection tends to decrease due to the scaling relations given above. Fabry-Perot oscillations are not expected to limit the bandwidth, since from Eq. 9 $\Delta\omega_{\mathrm{FP}}/\omega \approx 0.02$, or $\Delta\omega_{\mathrm{FP}}/2\pi \approx 4$ THz.

#8019 - $15.00 USD
Received 6 July 2005; revised 24 August 2005; accepted 29 August 2005

7. Dispersion Compensation

Signal dispersion can be compensated by using a sequence of two tapered gratings, as shown in Fig. 7. The light first travels through a grating with period a_1, where a_1 and the other structural parameters are chosen to place the operating frequency at the edge of the lowest band, which has negative curvature. A small decrease in the grating refractive index will raise the lowest band, increasing the group velocity. After traveling through the grating, the light enters a second grating with period a_2. a_2 is chosen larger than a_1, such that the operating frequency falls in the upper band, which has negative curvature. A small increase in the grating refractive index will shift the upper band down, again increasing the group velocity. The net effect of tuning the two regions is an increase in the total group velocity. Dispersion compensation is a standard practice in optical-fiber communication systems [2] and Fiber Bragg Gratings [24]. Similarly here, it is clear that for either the shifted or unshifted band, choosing the dispersion coefficient of the two gratings to be equal and opposite at the operating frequency ω_o yields a net zero-group-velocity-dispersion point for grating lengths $L_1 = L_2$. Residual pulse spreading is then governed by higher-order dispersion terms proportional to

$$\tilde{\beta}_3 = \frac{d}{d\omega}\left(\frac{d^2k_1}{d\omega^2} + \frac{d^2k_2}{d\omega^2}\right)\bigg|_{\omega_o} \approx \frac{3}{4\sqrt{\alpha}}\left(\frac{\Delta}{2}\right)^{-5/2}$$

within the quadratic band model, where $k_1(\omega)$ and $k_2(\omega)$ are the wave vectors of grating 1 and 2 respectively. Substituting the value of α from Section 5 above and setting $\Delta/2$ = 0.00454 ($2\pi c/a_1$), corresponding to a 4% separation of the band edge frequencies of the two gratings, gives a numerical value of 49.9 ps^3/m. Estimating the dispersion-limited length as $L < ((\Delta\omega/2\pi)^3\tilde{\beta}_3)^{-1}$, we find $L \approx 20$ m for a 100 GHz bandwidth.

A further quantity of interest is how the tunable delay $\Delta\tau$ varies across the bandwidth. Assume that gratings 1 and 2 are designed to have the same band-edge curvature (α) and to shift by the same amount $\delta\omega$ under tuning. We will center the operating bandwidth midway between the unshifted band edges, such that $\omega_o = (\omega_{\mathrm{be},1} + \omega_{\mathrm{be},2})/2$. Then the dispersion relations for the gratings may be written as

$$\omega_1(k_1) = \omega_o + \frac{\Delta}{2} - \alpha(\pi/a_1 - k_1)^2 \tag{11}$$

$$\omega_1'(k_1) = \omega_o + \frac{\Delta}{2} + \delta\omega - \alpha(\pi/a_1 - k_1)^2 \tag{12}$$

$$\omega_2(k_2) = \omega_o - \frac{\Delta}{2} + \alpha(k_2 - \pi/a_2)^2 \tag{13}$$

$$\omega_2'(k_2) = \omega_o - \frac{\Delta}{2} - \delta\omega + \alpha(k_2 - \pi/a_2)^2 \tag{14}$$

$$\tag{15}$$

where $\Delta/2 \equiv \omega_{\mathrm{be},1} - \omega_o = \omega_o - \omega_{\mathrm{be},2}$. (Small curvature corrections proportional to $\delta\alpha/\alpha << 1$ have been omitted for simplicity.) The total tunable time delay is given by

$$\Delta\tau = \frac{L}{2}\left[\Delta\left(\frac{1}{v_{g,1}}\right) + \Delta\left(\frac{1}{v_{g,2}}\right)\right] \tag{16}$$

where

$$\Delta\left(\frac{1}{v_{g,1}}\right) = \frac{1}{2\sqrt{\alpha}}\left[\frac{1}{\sqrt{\Delta/2 + \delta\omega - (\omega - \omega_o)}} - \frac{1}{\sqrt{\Delta/2 - (\omega - \omega_o)}}\right], \tag{17}$$

#8019 - $15.00 USD Received 6 July 2005; revised 24 August 2005; accepted 29 August 2005

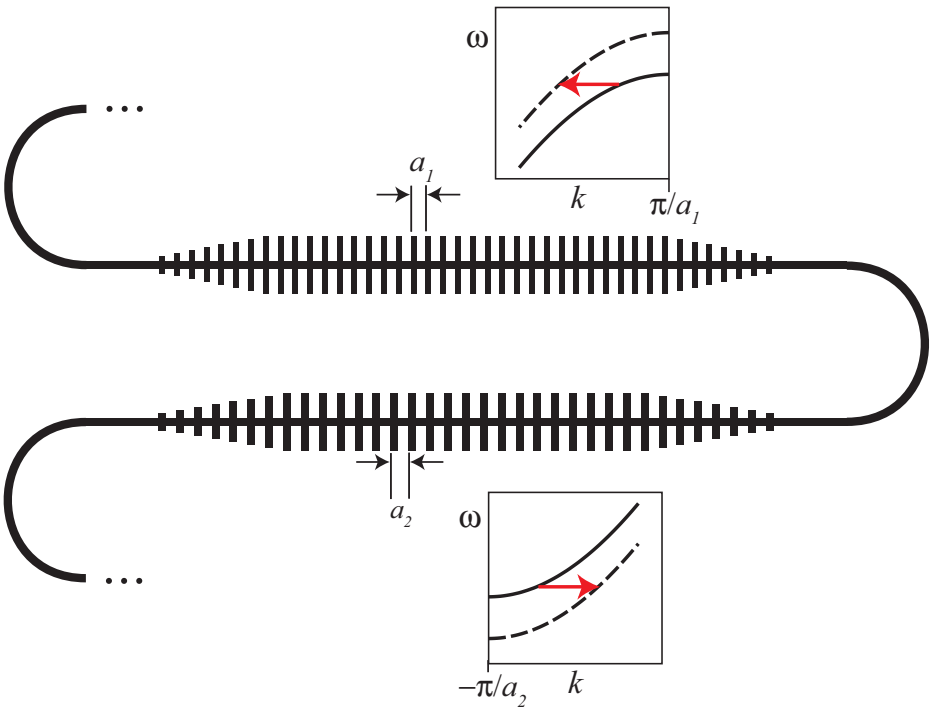

Fig. 6. Device design including adiabatically-tapered waveguide segments and dispersion compensation. Insets show the band diagram corresponding to each of the two grating regions.

$$\Delta\left(\frac{1}{v_{g,2}}\right) = \frac{1}{2\sqrt{\alpha}}\left[\frac{1}{\sqrt{\Delta/2+\delta\omega-(\omega_o-\omega)}} - \frac{1}{\sqrt{\Delta/2-(\omega_o-\omega)}}\right], \tag{18}$$

and $L = L_1 + L_2$, with $L_1 = L_2$ from the dispersion compensation condition above.

In Fig. 7 we plot the dispersion-compensated tunable delay per unit length, $\Delta\tau/L$ as a function of frequency. $\Delta\tau/L$ is shown in units of c, the speed of light, and the frequency is expressed in dimensionless units as $(\omega-\omega_o)/(\Delta/2)$. (All time delays are negative due to our convention that the unshifted band has lower group velocity.) The time delay due to grating 1 alone, shown by the red, dashed line, diverges at the upper end of the frequency range, where $\omega \to \omega_{\mathrm{be},1}$ and $(\omega-\omega_o)/(\Delta/2) = 1$. At lower frequencies, away from the band edge, the time delay approaches a constant. Meanwhile, the time delay due to grating 2 alone, shown by the blue, dashed-dotted line, diverges at the lower end of the frequency range at the band edge of grating 2. The average delay, which enters Eq. 16, diverges at both band edges and is flat across the center of the band, giving a constant time delay. The value is equal to

$$\Delta\tau/L = \frac{1}{2\sqrt{\alpha}}\left[\frac{1}{\sqrt{\Delta/2+\delta\omega}} - \frac{1}{\sqrt{\Delta/2}}\right] \approx -0.8503c^{-1}. \tag{19}$$

In physical units, this corresponds to a tunable delay of 2.834 ns per meter of device length. The variation in tunable delay per unit length is, moreover, less than 0.03% across a 100 GHz bandwidth ($|(\omega-\omega_o)/(\Delta/2)| < 0.0128$) and less than 3% across a 1 THz bandwidth.

For simplicity, we have assumed that the two gratings are designed to have the same curvature α and length L. For gratings with differing curvature values α_1 and α_2, the dispersion compen-

#8019 - $15.00 USD Received 6 July 2005; revised 24 August 2005; accepted 29 August 2005

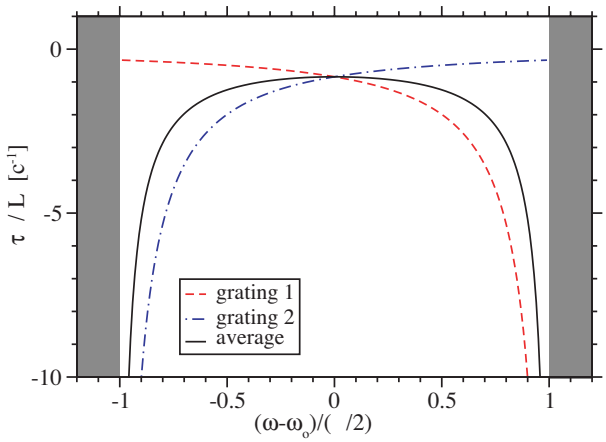

Fig. 7. Effect of dispersion compensation on the tunable time delay. Using grating 1 or grating 2 alone causes the tunable delay to vary strongly across the bandwidth. Cascading the two gratings as in Fig. 7 (labeled "average") gives a flat tunable delay in the center of the bandwidth.

sation condition is determined by the relation $L_1\beta_{2,1}+L_2\beta_{2,2}=0$, where $\beta_{2,i}=d^2k_i/d\omega^2$, with the result that L_1 and L_2 should be chosen to satisfy $L_1/\sqrt{\alpha_1}=L_2/\sqrt{\alpha_2}$. It is easily shown by straightforward modification of the equations above that the same condition will guarantee a flat tunable delay at the center of the bandwidth. Throughout, we assume that $\delta\omega_1=\delta\omega_2$. This frequency shift is related to the index shift as $\delta\omega/\omega=-\delta n\sigma/n$, where σ is the fraction of the modal field energy in dielectric [25], and so the indices of the two gratings will generally have to be tuned by different amounts to achieve identical shifts in frequency.

Lastly, we note that while the quadratic band model serves as a useful model for understanding physical trends and guiding design, fine-tuning of experimental designs will presumably require direct calculations of the grating band structures. Defining a relative error arising from the non-quadraticity of the band as $(\alpha-\alpha_{\rm eff}(\omega))/\alpha$, where $\alpha_{\rm eff}(\omega)=v_g/2(\pi/a-k)$, we find that the error can be as large as 10% for a 2% detuning from the band edge.

8. Maximum achievable tunable time delays

To determine the maximum tunable time delays achievable in slow-light, band-edge waveguides, we must consider how close to the band edge a device can be operated in practice. Imperfections in fabricated devices can be attributed to two main effects: (1) systematic deviations in actual feature sizes from their designed values, typically introduced during the e-beam patterning stage, and (2) random deviations in feature sizes along the device as a result of roughness, typically introduced during the etch stage. Assuming that the systematic deviations can be controlled through careful design and process development, the random deviations will ultimately limit device performance. As a rough rule of thumb, operating within x% of the band edge should require an accuracy of x% of the minimum feature size. For the device modeled above, for example, operating within 4% of the bandwidth requires 6 nm accuracy, and should be achievable using existing fabrication methods. Operating within 1% of the band edge would require an accuracy of 1.5 nm. While more challenging, analysis of fabricated Si/air structures has already shown that the rms roughness can be reduced to this range [26]. Future improvements in fabrication techniques and/or alternate fabrication methods could further re-

#8019 - $15.00 USD Received 6 July 2005; revised 24 August 2005; accepted 29 August 2005

duce achievable tolerances.

For a given distance from the band edge, we can extrapolate from typical loss values to estimate the achievable tunable delay time. It can be shown from coupled-mode theory [23, 27, 28] or from Green's function arguments [29] that radiation losses in periodic waveguides scale as $1/v_g$, where v_g is the group velocity of the mode, while reflection losses scale as $1/v_g^2$. Given typical measured loss values for grated structures, we can obtain an approximate upper bound on the slow-light loss by multiplying by a factor of $(1/v_g^2)/(1/v_{g,\mathrm{meas}}^2)$, where $v_{g,\mathrm{meas}}$ is the group velocity of the mode for which the measured loss value is given, typically near $c/n_{\mathrm{Si}} \approx c/3.45$. We will estimate the maximal device length as the $1/e$ decay length of power in the waveguide mode for the unshifted band, which has the lowest group velocity. This length can then be used to obtain a maximum tunable time delay from the calculation of Fig. 3 along with the linear dependence of $\Delta\tau$ on L. For simplicity, we do not explicitly consider variations in loss between the regular and dispersion-compensating section of the device, which we expect to be small, and estimate the total tunable time delay from the loss characteristics of the regular grating.

For operation at 4% away from the unshifted band edge ($\Delta\omega_{\mathrm{be}}/\omega_{\mathrm{be}} = 0.04$), the group velocity of the unshifted band is $\approx 0.20c$. Loss measurements for tightly-confined, photonic-crystal waveguides yield values in the range of 1 dB/mm [30]. Multiplying this value by the group-velocity enhancement factor yields a slow-light loss of roughly 2.1 dB/mm. We obtain the $1/e$ decay length from the expression

$$L_{1/e} = \frac{-10\log_{10}(1/e)}{\text{loss in dB/mm}} = \frac{4.3429\,\mathrm{dB}}{2.1\,\mathrm{dB/mm}} = 2.1\,\mathrm{mm}.$$

From Fig. 3, we infer that this length gives a tunable time delay of approximately 2 ps. For operation at 1% from the band edge ($\Delta\omega_{\mathrm{be}}/\omega_{\mathrm{be}} = 0.04$), $v_g = 0.113$, and the estimated loss increases to 6.6 dB/mm. $L_{1/e}$ decreases to 0.66 mm, but due to the enhanced sensitivity closer to the band edge, the tunable delay time increases slightly to 3 ps.

Reduction of the loss value in dB/mm significantly increases the delay time. A loss of 0.1 dB/mm in our structure increases the decay length by a factor of 10, for tunable time delays in the 20-30 ps range. Oxidation smoothing techniques have demonstrated experimental loss reductions of a factor of 4 in dB/length [31]. Clearly, a willingness to tolerate higher power penalties in the device ($>$ -4.3 dB) will also increase the achievable tunable delay.

Another route to reduced loss is modal delocalization. Designing the waveguide to have lower modal amplitude at the sidewalls will reduce scattering losses due to surface roughness [32]. However, modal delocalization also tends to decrease the size of the band gap, which via Eq. 6 will increase the required device length for a given time delay. Optimization of this tradeoff is a promising route for further inquiry.

9. Comparison to other on-chip time delays

The figures of merit defined in this paper also apply to other tunable time-delay device schemes, and a systematic comparison will prove helpful in evaluating their relative merits. While such analyses are beyond the scope of this paper, we comment briefly on similarities and differences of the proposed schemes below. We note that while it has been suggested that band-edge devices should be extraordinarily sensitive to disorder [8], disorder is a problem for *any* slow-light device, due to the group-velocity scaling arguments discussed above. We emphasize that the scaling argument applies quite generally to a wide range of slow-light devices, whether operated in transmission or reflection, and for arbitrary periodic geometries.

The most similar proposal to that presented here is the use of chirped photonic-crystal waveguides discussed in Ref. [15]. In this case, the waveguide chirping compensates the group-

#8019 - $15.00 USD Received 6 July 2005; revised 24 August 2005; accepted 29 August 2005

velocity dispersion. Alternately, light may be transferred from an initial chirped grating to a second grating with opposite dispersion sign. As in the scheme we propose here, achievable delay times are ultimately limited by waveguide loss near the band edge. Tuning such a device will require external control of the grating chirp by imposition of a spatial refractive index gradient across the device.

A second class of proposed devices use waveguides coupled to microcavities/microresonators. Such devices are ultimately limited by the cavity quality factor, Q. The highest reported Q's for on-chip, high-index-contrast cavities (e.g. Si/air) are 100,000 for photonic-crystal slab cavities [33] and 139,000 for microring resonators [34]. The decay time of the optical power in the cavity mode will limit the maximum achievable time delay. In a time $T = Q/\omega_o$, the optical power decays by $1/e$, where ω_o is the center frequency of the optical pulse. Q's in the 100,000–139,000 range correspond to decay times of 80 ps–111 ps at a wavelength of 1.55 μm. In comparison, achieving the same decay time in a waveguide structure requires waveguide loss values in the 0.6–0.45 dB/mm range, where it is assumed that the loss measurement is taken at group velocities near $c/n_{\mathrm{Si}} \approx c/3.45$.

While higher cavity Q's are available in silica material systems, e.g. $Q > 10^8$ in fused silica microspheres and microtorii, such resonators do not currently lend themselves to on-chip integration of multiple resonators/cavities and waveguides. A recent paper, however, has demonstrated large tunable delays (up to 320 ps per stage) in the lower-index-contrast regime using silica ring resonators (2% index contrast) [3].

We note that tunable delays based on coupled waveguide-cavity systems generally require spatially-localized tuning mechanisms on the micron scale (e.g. optical, electrical, or thermal) to separately control the resonance frequencies of individual waveguides and cavities, as in [12]. Further tuning may be required to trim out fabrication-related errors in the individual cavity frequencies. In comparison, the design we propose here would require separate tuning of the two millimeter-scale regions that contain the regular and dispersion-compensating gratings.

10. Conclusion

We have shown that grated waveguides operated in transmission near a photonic band edge enhance the tunability of a time-delay device. The enhancement is due to slow light speeds near the band edge, which result in a large change of group velocity for a small change in index and hence a shorter device length. Explicit numerical calculations for a realistic grating verify that figures of merit for the device are well predicted from a simple quadratic band model. Using coupled-mode theory, we have shown that optimized tapers can be designed that achieve very low reflection in short lengths, even at slow group velocities. Cascading two tapered gratings both compensates signal dispersion and gives rise to a flat tunable time delay across the operating bandwidth. Estimates of the tunable delay are comparable with other proposed high-index-contrast, on-chip devices. Optimization, fabrication, and optical characterization of slow-light structures are ongoing [35].

Acknowledgments

The authors thank S. J. Spector, M. W. Geis, R. C. Williamson, T. Lyszczarz, M. Soljačić, and Shanhui Fan for helpful discussions and suggestions. This work was supported by the Defense Advanced Research Projects agency under Air Force Contract #F19628-00-C-0002 and the Materials Research Science and Engineering Center program of the National Science Foundation under Award No. DMR-9400334. Opinions, interpretations, conclusions, and recommendations are those of the authors, and not necessarily endorsed by the United States Government.